Interreflection Removal Using Fluorescence

Ying Fu[1], Antony Lam[2], Yasuyuki Matsushita[3],
Imari Sato[4], and Yoichi Sato[1]

[1]The University of Tokyo, [2]Saitama University,
[3]Microsoft Research Asia, [4]National Institute of Informatics

Abstract. Interreflections exhibit a number of challenges for existing shape-from-intensity methods that only assume a direct lighting model. Removing the interreflections from scene observations is of broad interest since it enhances the accuracy of those methods. In this paper, we propose a method for removing interreflections from a single image using fluorescence. From a bispectral observation of reflective and fluorescent components recorded in distinct color channels, our method separates direct lighting from interreflections. Experimental results demonstrate the effectiveness of the proposed method on complex and dynamic scenes. In addition, we show how our method improves an existing photometric stereo method in shape recovery.

Keywords: Fluorescence, bispectral model, bispectral interreflection model, and interreflection removal
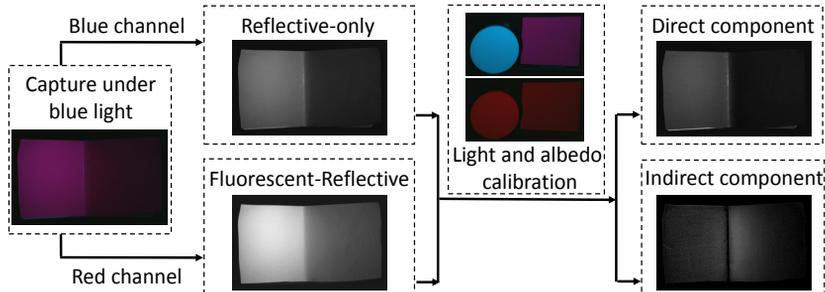
1   Introduction

Interreflection is a global light transport process whereby light reflected from a surface point illuminates other points. In the presence of interreflections, an intensity observation of a scene consists of the directly reflected light rays after a single-bounce on a surface (direct component) and light rays that bounce off of the scene surface multiple times before they reach the camera (indirect component). Modeling and removing interreflections is of broad interest for making shape-from-intensity methods to work properly, because most of them are designed to take only the direct component as input.

Recent studies on this problem provide deeper understandings about the inverse light transport and show that the direct and indirect components can be separated for static scenes image [23, 18, 15]. In addition, some papers have tackled the problem for dynamic scenes but the capture process may require specialized masks [18, 20] or motion compensation [1].

In this paper, we show that separation can be achieved for dynamic scenes by capturing only a single image using *fluorescence* (see Fig. 1). Fluorescent materials[1] not only reflect incident light but also absorb and emit light at longer

---

[1] In practice, fluorescent materials show both ordinary reflection and fluorescent emission.

Fig. 1. Overview of the proposed method. A fluorescent object is captured under blue light, whose blue channel is a reflective-only image and red channel is a wavelength-shifted fluorescent-reflective image. The lighting and albedo are calibrated by images of the flat white target and fluorescent sheet captured under blue and red light. After calibration, direct and indirect components can be recovered.
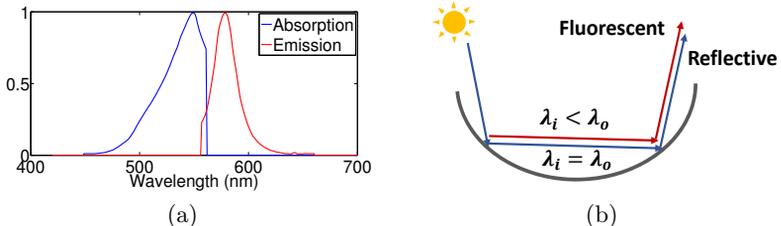
wavelengths [13] (see Fig. 2) . This physical property allows us to obtain single-shot images that contain reflective-only images at the same wavelength as the illuminant and wavelength-shifted images that are a mixture of fluorescent emission and interreflections of those emissions. We call this wavelength-shifted image a fluorescent-reflective image. We illustrate these concepts with an example. If a scene is illuminated by a blue light source, the reflective-only image is recorded in the blue channel, and the fluorescent-reflective image could be captured in the red channel (see Fig. 1). Interreflections still exist in both channels but using this bispectral measurement, we develop a direct-indirect decomposition method by deriving a new interreflection model for fluorescence and extending Liao *et al.* [15] where they used varying light colors and multiple images. Unlike Liao *et al.*'s method, our method only requires a single image with an assumption of commonly available fluorescent materials, which enables interreflection removal from a dynamic scene.

In summary, our main contributions are that we

- derive a general interreflection model for fluorescent materials,
- develop a method to separate direct-indirect components from reflective-only and fluorescent-reflective measurements, and
- show that a single-shot measurement is sufficient for the decomposition using fluorescence.

2   Related Work

Fluorescence Fluorescent analysis has received attention in recent years in computer vision. Examples of such work can be found in color rendering [11, 25], reflectance and re-radiation modeling [10], camera spectral sensitivity estimation [8], 3D reconstruction [21, 24], immersion range scanning [9], and color relighting of real scenes [4, 14]. In many of these methods, a phenomenon of fluorescence known as Stokes shift is exploited to achieve results. Specifically, Stokes

Fig. 2. (a) An example of absorption and emission spectra in the McNamara and Boswell fluorescence spectral dataset [16]. (b)When the fluorescent material is illuminated, it will reflect at the same wavelength and emit light at longer wavelengths.

shift can be described simply as the absorption of light at shorter wavelengths and emission of light at longer wavelengths [13]. The way this works is that when incident light hits a fluorescent surface, the surface's absorption spectrum will determine how much of the light is absorbed. Some of the absorbed energy is then released in the form of an emission spectrum at longer wavelengths than the incident light. The remainder of the absorbed energy is released as heat. In this paper, we take advantage of Stokes shift to assist with interreflection removal.

Interreflection   There have been a number of methods that analyze interreflection and demonstrate applications such as shape recovery. Koenderink and Doorn [12] presented a general model for diffuse interreflections. Forsyth *et al.* [3, 2] studied how interreflections affect shape recovery. Later, Nayar *et al.* [19] addressed the interplay between interreflections and shape by iteratively refining the shape and reflectance of surfaces. They then extended their algorithm to colored and multi-colored surfaces [17].

Despite the effectiveness of past approaches such as [19] and [17], the modeling and separation of interreflections is of broader interest because most shape-from-intensity methods assume only direct lighting. Thus solving the problem of separating out interreflections would allow for improving an entire body of methods in the literature. An early example of such work was presented by Funt *et al.* [5, 6] where the color different effect in interreflections was used to separate interreflections from direct lighting. Later, Seitz *et al.* [23] proved the existence of an inverse light transport operator capable of separating m-bounced light from scenes with uniform albedo and Lambertian surfaces. However, their method requires a laser and scene capture is very time consuming. In addition, their method is not robust to complex shapes. Nayar *et al.* [18] were able to separate direct and global lighting components for complex scenes using spatially high frequency illumination. In principle, their method would be very fast but in practice, they require additional images or reduced resolution.

More recently, Liao *et al.* [15] removed interreflections by using spectrum-dependent albedo in scenes but their method still needs two images captured under different illuminations. In this paper, we show that by exploiting properties of fluorescence, interreflections can be removed using only using one color image under one illumination. Our method also does not require a highly specialized setup and images can be captured using a standard RGB camera in a straightforward manner. This provides an advantage over other methods for in-

terreflection removal on dynamic scenes that need more specialized setups such as masks [18, 20] or motion compensation [1]. Like Liao *et al.* [15], our main drawback is that the object needs to be homogeneously colored with the reflective and fluorescent component. However, even when an object does not satisfy this condition, it is possible to color it using commonly available paint.

3   Bispectral Model for Interreflection Removal

In this section, we first introduce the bispectral model for fluorescent materials. We then briefly review the interreflection model for ordinary reflective materials with a uniform albedo and Lambertian surface and derive the interreflection model for fluorescence. After that, we present our model to separate direct and indirect lighting based on fluorescence. Finally, we describe the practical issues of lighting and albedo calibration.

3.1   Bispectral Model

In general, the appearance of fluorescent materials consists of both reflective and fluorescent components [22]. If we assume a Lambertian surface, the local reflection of the reflective component can be described as

$$E_r(x, \lambda) = \rho(x, \lambda)L(\lambda)\cos\theta, \tag{1}$$

where $\rho(x, \lambda)$ is the albedo of the surface point x at wavelength λ, $L(\lambda)$ is the incoming radiance from the light source, and θ is the angle between the surface normal and light source directions. We refer to $\rho(x, \lambda)$ as the *reflective albedo*.

   Unlike the reflective component that reflects light rays at the same wavelength as the incident light, the fluorescent component absorbs and emits light at different wavelengths from the incident one [25, 10, 22]. Another interesting property is that, as shown by Glassner [7], fluorescence emissions have no directional characteristics and are uniformly radiated in all directions. In other words, fluorescence emissions behave like light reflected from a Lambertian diffuse surface. Therefore, the outgoing radiance E_f from a fluorescent material under the light $L(\lambda_i)$ can be written as

$$E_f(x, \lambda_i, \lambda_o) = \eta(x, \lambda_i, \lambda_o)L(\lambda_i)\cos\theta, \tag{2}$$

where λ_i and λ_o represent the incident and outgoing wavelengths, respectively, and $\eta(x, \lambda_i, \lambda_o)$ is a direction-invariant function that describes the re-radiation property of the fluorescence. According to the characteristics of fluorescence [22], $\eta(x, \lambda_i, \lambda_o)$ can be factored as

$$\eta(x, \lambda_i, \lambda_o) = \mu(x, \lambda_o)a(x, \lambda_i), \tag{3}$$

where $a(x, \lambda_i)$ and $\mu(x, \lambda_o)$ define the absorption and emission factors of the fluorescent material, respectively. In the following, we call $\mu(x, \lambda_o)$ the *fluorescent albedo*. The incoming radiance energy is absorbed by $a(x, \lambda_i)$ as $\int a(x, \lambda_i)L(\lambda_i)d\lambda_i$; therefore, Eq. (2) can be rewritten as

$$E_f(x, \lambda_o) = \mu(x, \lambda_o)\left(\int a(x, \lambda_i)L(\lambda_i)d\lambda_i\right)\cos\theta. \tag{4}$$

Finally, the observation $E(=E_r+E_f)$ becomes

$$E(x,\lambda_o) = \left[\rho(x,\lambda_o)L(\lambda_o)\delta(\lambda_i-\lambda_o) + \mu(x,\lambda_o)\int a(x,\lambda_i)L(\lambda_i)d\lambda_i\right]\cos\theta, \quad (5)$$

in which E_r and E_f are independently observed at two distinct wavelengths λ_i and λ_o, respectively. The delta function $\delta(\lambda_i-\lambda_o)$ is associated with the reflective component because an ordinary reflective component only reflects light at the same wavelength as its incident light ($\lambda_i = \lambda_o$).

3.2 Bispectral Interreflection Model

We briefly review the interreflection model for the ordinary reflective component on a Lambertian surface [12] and extend the interreflection model for the fluorescent component.

Interreflection model for reflective component. The interreflection geometry [12] between points $x \in \mathbb{R}^3$ and $x' \in \mathbb{R}^3$ is described by a kernel K as

$$K(x,x') = \frac{Pos[n(x)^T(x'-x)]Pos[n(x')^T(x-x')]}{\|x'-x\|^2}, \quad Pos[a] = \frac{a+|a|}{2}, \quad (6)$$

where $n(x) \in \mathbb{R}^3$ is the surface normal at point x. The outgoing radiance of the reflective component $I_r(x,\lambda)$ can be expressed as the sum of direct and indirect components as

$$I_r(x,\lambda) = \frac{\rho(x,\lambda)}{\pi}P(x,\lambda) + \frac{\rho(x,\lambda)}{\pi}\int K(x,x')I_r(x',\lambda)dx', \quad (7)$$

where $P(x,\lambda)$ is the irradiance from the light source towards the surface point x at wavelength λ. By defining iterated kernels K_m as

$$K_1(x,x') = \frac{K(x,x')}{\pi}, \quad K_m(x,x') = \int \frac{K(x,y)}{\pi}K_{m-1}(y,x')dy \ (m>1), \quad (8)$$

Eq. (7) can be rewritten as the polynomial function of ρ as

$$I_r(x,\lambda) = \rho(x,\lambda)\frac{P(x,\lambda)}{\pi} + \sum_{m=2}^{\infty}\rho^m(x,\lambda)\int K_{m-1}(x,x')\frac{P(x',\lambda)}{\pi}dx'. \quad (9)$$

By defining

$$R_1(x,\lambda) = \frac{P(x,\lambda)}{\pi},$$
$$R_m(x,\lambda) = \int K_{m-1}(x,x')\frac{P(x',\lambda)}{\pi}dx' \quad (m>1), \quad (10)$$

Eq. (9) becomes

$$I_r(x,\lambda) = \sum_{m=1}^{\infty}\rho^m(x,\lambda)R_m(x,\lambda). \quad (11)$$

as described in [15]. Interested readers can refer to [12], [19] and [15] for more details.

Interreflection model for fluorescent component. Analogous to interreflections of the reflective component, the direct component of the fluorescent component is

$$\mu(x, \lambda_o) \frac{\int a(x, \lambda_i) P(x, \lambda_i) d\lambda_i}{\pi}. \tag{12}$$

From Eq. (6), we can see that the interreflection geometry $K(x, x')$ is independent of the albedo of the objects and the energy absorbed from the light source. Also, the fluorescence emissions are typically not re-absorbed by the same fluorescent material again[2]; therefore, the interreflection of fluorescence emissions behaves like that of the reflective components except for the initial emission. Therefore, the second-bounce component can be written as

$$\mu(x, \lambda_o) \rho(x, \lambda_o) \int K_1(x, x') \frac{\int a(x', \lambda_i) P(x, \lambda_i) d\lambda_i}{\pi} dx', \tag{13}$$

where $\rho(x, \lambda_o)$ is the reflective albedo at the outgoing wavelength λ_o. The radiance of the fluorescent component at surface point x is, therefore represented as the sum of the direct component and interreflections as

$$I_f(x, \lambda_o) = \mu(x, \lambda_o) \frac{\int a(x, \lambda_i) P(x, \lambda_i) d\lambda_i}{\pi} + \\ \sum_{m=1}^{\infty} \mu(x, \lambda_o) \rho^m(x, \lambda_o) \int K_m(x, x') \frac{\int a(x', \lambda_i) P(x, \lambda_i) d\lambda_i}{\pi} dx'. \tag{14}$$

By defining

$$F_1(x, \lambda_i) = \frac{\int a(x, \lambda_i) P(x, \lambda_i) d\lambda_i}{\pi}, \\ F_m(x, \lambda_i) = \int K_{m-1}(x, x') \frac{\int a(x', \lambda_i) P(x, \lambda_i) d\lambda_i}{\pi} dx', \ (m > 1), \tag{15}$$

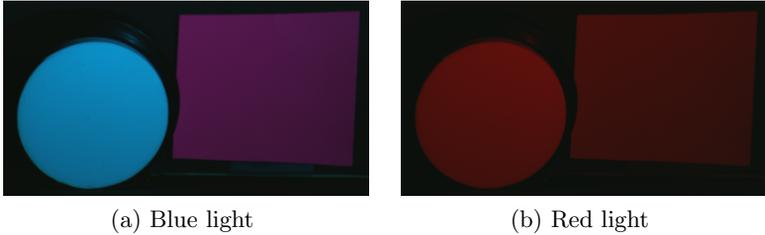the interreflection model for the fluorescent component can be written as

$$I_f(x, \lambda_o) = \mu(x, \lambda_o) F_1(x, \lambda_o) + \sum_{m=1}^{\infty} \mu(x, \lambda_o) \rho^m(x, \lambda_o) F_{m+1}(x, \lambda_o). \tag{16}$$

Unlike the conventional interreflection model for the reflective component (Eq. (11)), the derived model includes both fluorescent and reflective albedos at the outgoing wavelength λ_o.

3.3 Separation of Direct and Indirect Components

In theory, one would need an infinite-bounce model to fully describe interreflections. Fortunately, in practice, a 2-bounce model is sufficient for accurately modeling interreflections [6]. We thus restrict our attention to the 2-bounce case. If

---

[2] The overlap between absorption and emission spectra is small. As a result, only a negligible amount of emitted light is re-absorbed.

(a) Blue light   (b) Red light
Fig. 3. Lighting and albedo calibration.

we observe the reflective component at the same wavelength ($\lambda_i = \lambda_o$) as the illumination, we obtain

$$I_r(x, \lambda_i) = \rho(x, \lambda_i)R_1(x, \lambda_i) + \rho^2(x, \lambda_i)R_2(x, \lambda_i). \qquad (17)$$

The fluorescent component can be observed at a longer wavelength as

$$I_f(x, \lambda_i, \lambda_o) = \mu(x, \lambda_o)F_1(x, \lambda_i) + \mu(x, \lambda_o)\rho(x, \lambda_o)F_2(x, \lambda_i). \qquad (18)$$

For convenience, we remove λ_i and λ_o in all functions in Eqs. (17) and (18) and use ρ_1 and ρ_2 to represent the reflective albedo at incident wavelength λ_i and outgoing wavelength λ_o, respectively. We also assume that the scene consists of a uniform material, so the albedos $\rho(x)$ and $\mu(x)$ will be the same for all points x and can be represented as ρ and μ. Therefore, Eqs. (17) and (18) can be rewritten as

$$I_r(x) = \rho_1 R_1(x) + \rho_1^2 R_2(x), \quad I_f(x) = \mu F_1(x) + \mu\rho_2 F_2(x). \qquad (19)$$

As will be detailed in Sec. 3.4, we condition $P(x, \lambda_i) = \int a(x, \lambda_i)P(x, \lambda_i)d\lambda_i$ so $R_m(x) = F_m(x)$(m=1,2). Thus Eq. (19) can then be written as

$$\begin{bmatrix} I_r(x) \\ I_f(x) \end{bmatrix} = \begin{bmatrix} \rho_1 & \rho_1^2 \\ \mu & \mu\rho_2 \end{bmatrix} \begin{bmatrix} R_1(x) \\ R_2(x) \end{bmatrix}. \qquad (20)$$

We later detail how ρ_1, ρ_2 and μ can be determined but provided they are known, we can solve for $R_1(x)$ and $R_2(x)$ in Eq. (20) by a matrix inverse. From this, $\rho_1 R_1(x)$ and $\mu R_1(x)$ would give us the direct component in the reflective and fluorescent parts respectively.

Compared with [15], our method requires one less image to capture. Since the 2-bounce model can accurately approximate interreflections in practice, our method can remove interreflections only with a single image. As demonstrated in later in experiments, this allows the interreflection removal of a dynamic scene by the straightforward recording of a video using a standard RGB camera.

3.4   Lighting and Albedo Calibration

The equality $R_m(x) = F_m(x)$ holds only if $P(x, \lambda_i) = \int a(x, \lambda_i)P(x, \lambda_i)d\lambda_i$, which is not the general case. Furthermore, in order to solve Eq. (20), the value of the albedos are required. We will address these two issues in the following.

Light Intensity Calibration As in Eq. (19), $R_m(x) = F_m(x)$ only when irradiance $P(x, \lambda_i)$ is equal to $A(x) = \int a(x, \lambda_i) P(x, \lambda_i) d\lambda_i$. To make these two values equal, we would need to calibrate the fluorescent absorption spectrum and control the light source carefully. This would be technically very challenging so we instead use a simpler calibration procedure. Let us assume $P(x, \lambda_i)$ is α times $A(x)$, then for every surface point x, the radiance $L(\lambda_i)$ from the light source for the reflective component is also α times the absorbed energy $\int a(\lambda) L(\lambda_i) d\lambda_i$ for the fluorescent component with uniform albedo. That is,

$$\alpha = \frac{P(x, \lambda_i)}{\int a(x, \lambda_i) P(x, \lambda_i) d\lambda_i} = \frac{L(\lambda_i)}{\int a(\lambda_i) L(\lambda_i) d\lambda_i}. \tag{21}$$

Because of this relation, we can calculate a single α for all points x. As defined in Eqs. (10) and (15), $R_m(x)$ and $F_m(x)$ are linearly dependent on the irradiance $P(x, \lambda_i)$ and $\int a(x, \lambda_i) P(x, \lambda_i) d\lambda_i$, respectively:

$$R_1(x) = \alpha F_1(x), \quad \text{and} \quad R_2(x) = \alpha F_2(x). \tag{22}$$

Therefore, Eq. (20) can be written as

$$\begin{cases} I_r(x) = \rho_1 R_1(x) + \rho_1^2 R_2(x) \\ I_f(x) = \frac{\mu}{\alpha} \left(R_1(x) + \rho_2 R_2(x) \right). \end{cases} \tag{23}$$

Albedo Ratio We discussed earlier that with known reflective albedos ρ_1 and ρ_2 and fluorescent albedo μ, we can solve for the direct and indirect lighting components. However, directly measuring these values is actually quite difficult. From from Eq. (1) and Eq. (4), reflective albedo ρ and fluorescent albedo μ can be described as

$$\rho(x, \lambda) = \frac{E_r(x, \lambda)}{L(\lambda) \cos \theta}, \quad \text{and} \quad \mu(x, \lambda_o) = \frac{E_f(x, \lambda_o)}{\left(\int a(x) L(\lambda_i) d\lambda_i \right) \cos \theta}. \tag{24}$$

Determining the albedos from Eq. (24) is difficult because we would need to know θ, the angle between the incident light and the surface normal.

Fortunately, a simple calibration procedure can be used to obtain albedo ratios which would also be sufficient for our purposes. If we take $\rho_1 R_1(x)$ and $\rho_1^2 R_2(x)$ as the unknown variables, Eq. (20) can be reformulated[3] as

$$\begin{bmatrix} I_r(x) \\ I_f(x) \end{bmatrix} = \begin{bmatrix} 1 & 1 \\ \frac{\mu}{\rho_1 \alpha} & \frac{\mu}{\rho_1 \alpha} \frac{\rho_2}{\rho_1} \end{bmatrix} \begin{bmatrix} \rho_1 R_1(x) \\ \rho_1^2 R_2(x) \end{bmatrix}. \tag{25}$$

Then measuring the relative surface albedo for a point x as opposed to the absolute value of the albedo can be simply done with the following ratios derived from Eq. (24)

$$\frac{\mu}{\rho_1 \alpha} = \frac{E_f(x, \lambda)}{E_{r1}(x, \lambda)}, \quad \text{and} \quad \frac{\rho_2}{\rho_1} = \frac{E_{r2}(x, \lambda)}{E_{r1}(x, \lambda)} \frac{L_1(\lambda)}{L_2(\lambda)}, \tag{26}$$

---

[3] The reformulation solves for scaled versions of $R_1(x)$ and $R_2(x)$ but this is still sufficient for analyzing direct and indirect lighting.

where L_1 and L_2 are blue and red lights respectively[4].

In the calibration process, the objects used to compute the albedo ratios should be made of the same material as the object under consideration, as well as being flat or convex to avoid any interreflections. As shown in Fig. 3, we usea flat fluorescent sheet and a spectrally flat white reflectance target to calibrate $\frac{\mu}{\rho_1\alpha}$ and $\frac{\rho_2}{\rho_1}$. The scene is captured under blue and red light. $\frac{E_f}{E_{r1}}$ is the ratio of the intensity of the fluorescent sheet in the blue and red channels under the blue light. $\frac{E_{r2}}{E_{r1}}$ is the ratio of the intensity of the fluorescent sheet in the red channel under the red light and the blue channel under the blue light. $\frac{L_1}{L_2}$ is the ratio of the intensity of the white target in the blue channel under the blue light and the red channel under the red light.

So far, the possibility to make Eq. (25) work is based on the assumption that the surface reflective albedo cannot be constant across the entire spectrum $(\rho_1 \neq \rho_2)$.
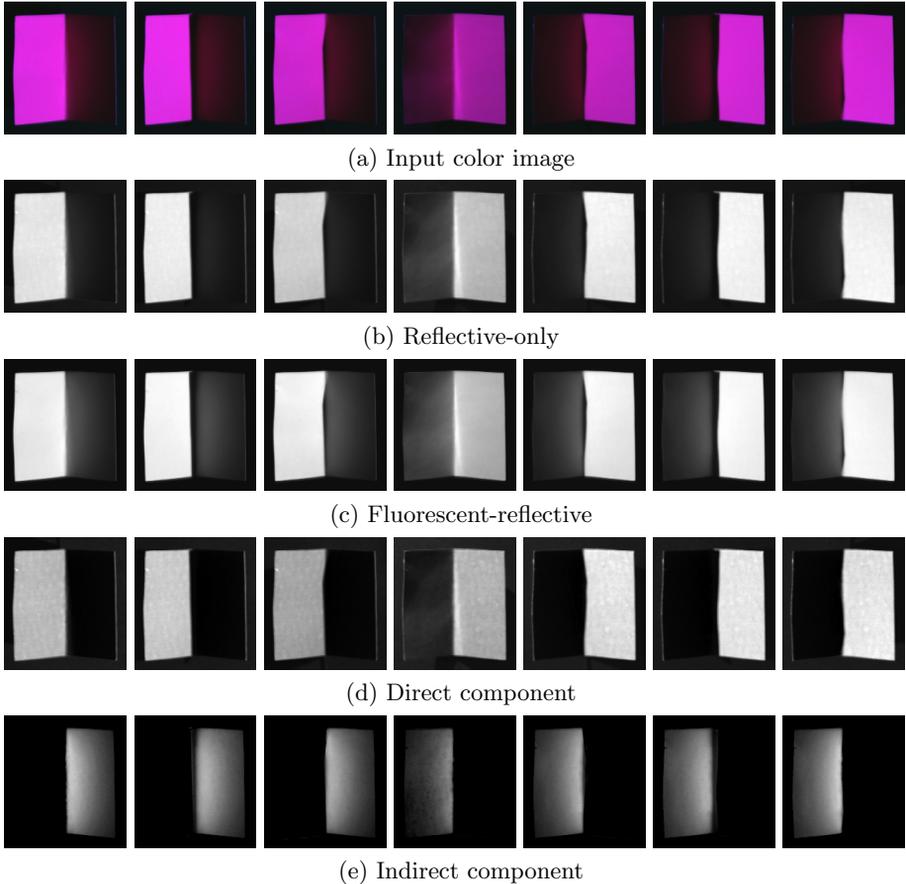
4   Experimental Results

We tested our method on real fluorescent objects. To obtain both reflective and fluorescent components effectively, we used pink fluorescent objects where the reflective component is strong in the blue channel and the fluorescent emission is strong in red channel. Such color characteristics make reflective-only and fluorescent-reflective capture ideal for use with a standard RGB camera. In practice, capture with other colors can also be done but different light sources or camera filters would be needed to remove some wavelengths so that reflective-only and fluorescent-reflective images can be captured. Our method requires all surface points to exhibit the same color. In a real application, objects could be easily spray painted. We could then get the benefits of our method's ability to separate direct and indirect components for moving objects. For our experiments, we used objects that naturally exhibit fluorescence and a leaf dish that was painted. These objects were all illuminated by blue light and captured in the blue and red channels of a CCD camera (SONY DXC-9000).

4.1   Separation Results

In this section, we show the results for the separation of direct and indirect components. We first give an overview of the entire process. As shown in Fig. 1, an RGB image is first captured under blue light. Since we used our pink fluorescent color, the blue channel is a reflective-only image while the red channel is a fluorescent-reflective image. As described in Sec. 3.4, the lighting and albedo are then calibrated by images captured under blue and red light, where the calibration targets are both flat. After calibration, direct and indirect components are recovered by Eq. (25).

Our first scene is a pink fluorescent v-shape object. The scene was first taken under blue light (Fig. 4 (a)). Its blue channel is then a reflective-only image
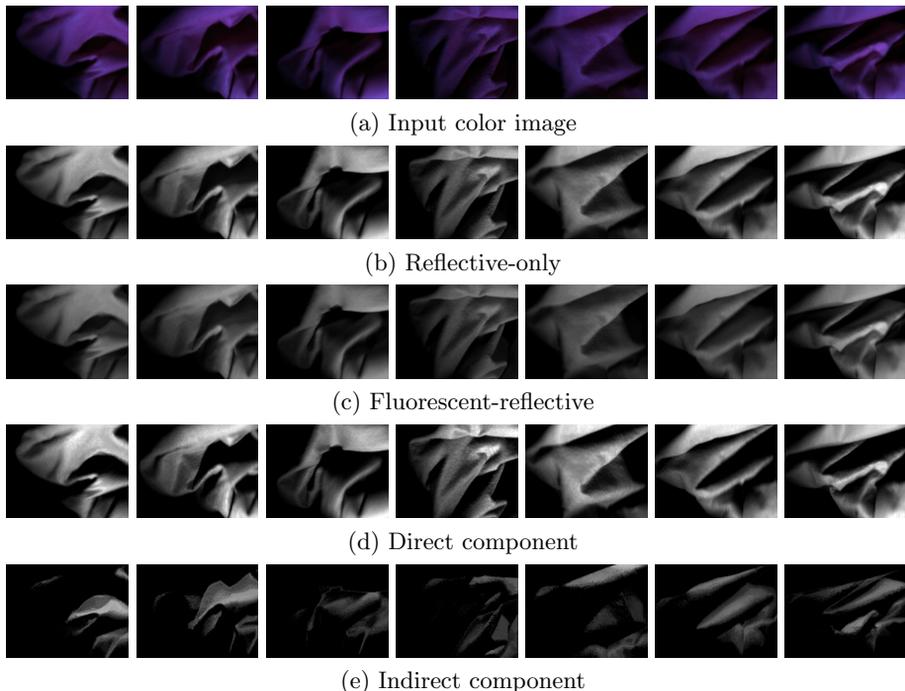
---

[4] In our method, L_1 should be in the short wavelength range, and L_2 should be the same appearance with the fluorescent emission spectrum so that it shows the spectral reflectance in the fluorescent emission area.

(a) Input color image

(b) Reflective-only

(c) Fluorescent-reflective

(d) Direct component

(e) Indirect component

Fig. 4. Separation results for the v-shape. (a) The input image captured under blue light. (b) The reflective-only image from (a)'s blue channel. (c) The fluorescent-reflective image from (a)'s red channel. (d) The separated direct component. (e) The separated indirect component.

(Fig. 4 (b)) and the red channel is a fluorescent-reflective image (Fig. 4 (c)). We calibrated the lighting and albedo by using the method in the previous section and found $\frac{\mu}{\rho_1 \alpha}$ and $\frac{\mu}{\rho_1 \alpha} \frac{\rho_2}{\rho_1}$ to be 1.10 and 2.07 for the pink fluorescent sheet, respectively. After calibration, the direct and indirect components were separated by Eq. (25) as shown in Fig. 4(d) and (e). In the figures, we have scaled the indirect component to $0 \sim 255$, for visualization purposes. We can see that when we light one side of the v-shape, the direct component is strong on one side while the indirect component is strong in other side. This observation fits our expectations of how interreflections would physically behave and demonstrates that our method removes interreflection effectively.

As mentioned, our method only requires a one-shot measurement to separate the direct and indirect component and so is applicable to dynamic scenes. In Fig. 5, seven successive video frames for a dynamic pink fluorescent cloth are

(a) Input color image

(b) Reflective-only

(c) Fluorescent-reflective

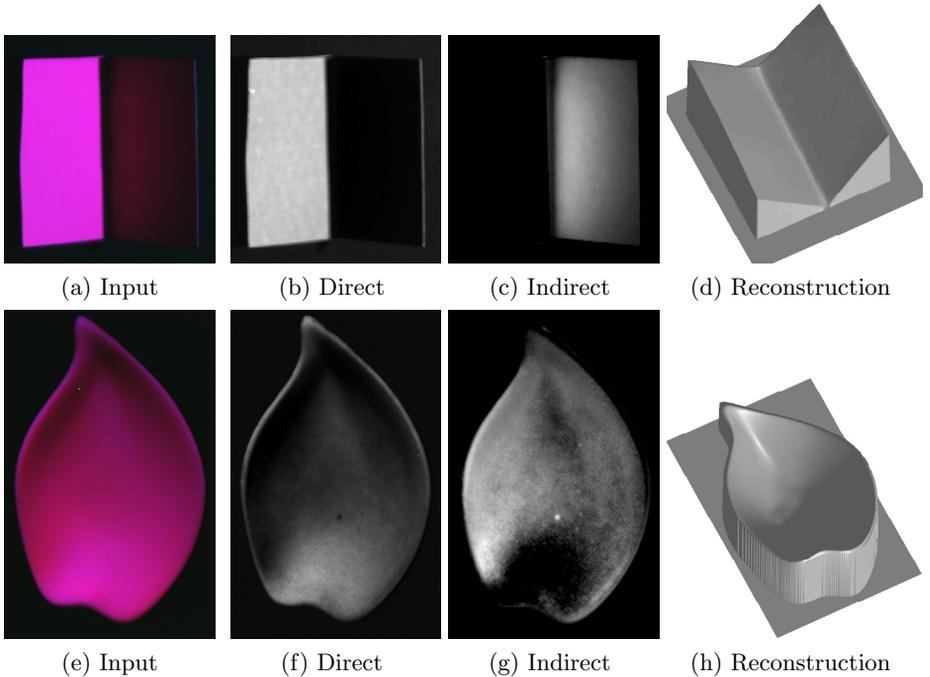(d) Direct component

(e) Indirect component

Fig. 5. Separation results for the moving fluorescent cloth. (a) The input image captured under blue light. (b) The reflective-only image from (a)'s blue channel. (c) The fluorescent-reflective image from (a)'s red channel. (d) The separated direct component. (e) The separated indirect component.

shown. We can see the changing of direct and indirect components in Fig. 5 (d) and (e) as a result of the object's motion. The direct component is strong in the flat area (Fig. 5 (d)) and the indirect component is strong in the wrinkled area. As with the v-shape, these observations fit our expectations of how interreflections would physically behave and demonstrates our method's effectiveness.

4.2   Photometric Stereo

To demonstrate a sample application and to further validate our separation results, we use the recovered direct component to perform photometric stereo [26]. We also tested using reflective-only and fluorescent-reflective images as inputs to photometric stereo and show our recovered direct component provides the best results. In our experiments, for each object, 12 images were captured with the object illuminated from different light source directions. The light source was about 1 m away from the object, which was $4 \sim 10$ cm in diameter.
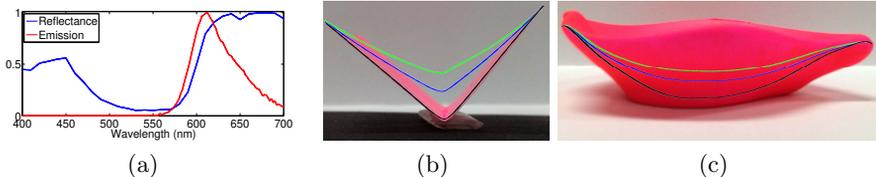
We tested our method on the pink fluorescent v-shape sheet and a "leaf dish". Fig. 6 shows one of the input images and the corresponding separated direct and indirect components. The surface normals were recovered by photometric stereo and the shape was integrated from the normal map. Fig. 6(d)(h) show the recovered shapes by using our recovered direct components.

| (a) Input | (b) Direct | (c) Indirect | (d) Reconstruction |

| (e) Input | (f) Direct | (g) Indirect | (h) Reconstruction |

Fig. 6. Reconstructed results for the fluorescent v-shape and leaf dish. (a)(e) One of the input images captured under the directional blue light. The corresponding separated direct and indirect components are shown (b)(f) and (c)(g). (d)(h) The recovered shape form the direct components.

In [19], Nayar *et al.* showed that interreflections cause recovered shapes to be shallow. We quantitatively show the improvement in using our interreflection removal method by comparing against recovered shape depths from using the reflective-only images and fluorescent-reflective images as inputs to photometric stereo.

We can see that the shape recovered from the fluorescent-reflective images (Fig. 7(b) green line) is more shallow than that from the reflective-only images(Fig. 7(b) blue line). This is because the reflectance spectrum is stronger in the red channel than in the blue channel (Fig. 7(a)). Recall that the fluorescent indirect component shown in Eq. (25), $\frac{\mu}{\rho_1\alpha}\frac{\rho_2}{\rho_1} = 2.07$ is greater than the reflective indirect component which is 1. Thus the indirect component $2.07\rho_1^2 R_2(x)$ in the fluorescent-reflective images is stronger than the $\rho_1^2 R_2(x)$ in the reflective-only images. From Fig. 7(a), we also see that the spectral reflectance has a strong overlap with the fluorescence emission spectrum. In the fluorescent photometric stereo work of [21] and [24], they both assume that spectral reflectance does not overlap with the fluorescent emission spectrum. This is not always the case and our method addresses situations where spectral reflectance does overlap with the fluorescent emission spectrum.

Fig. 7. (a) The reflectance and emission spectra for the fluorescent pink sheet. (b) and (c) The cross-sectional view of recovered shapes from fluorescent-reflective images (green line), reflective-only images (blue line) and direct components (dark line) superimposed into the side view of the v-shape and leaf dish, respectively.

Finally, the recovered shape from the direct component (Fig. 7(b) dark line) is deepest one, which indicates that our method removes the indirect component effectively. The ground truth angle between the two sides for the v-shape is about 90 degrees. The recovered angles for the shape from the direct component, reflective-only and fluorescent-reflective cases are 91, 101 and 114 degrees, respectively. Thus our recovered direct component provided a result very close to the ground truth. Similar results can be seen for the leaf dish in Fig. 7(c).

5   Conclusion

We presented a novel method for separating direct and indirect components using the phenomenon of fluorescence. By exploiting Stokes shift, we were able to observe separated reflective and fluorescent components simultaneously in two channels of an RGB camera. While both channels still contained interreflections, we devised a simple but effective decomposition method for separating out interreflections. From this, we derived a general interreflection model for fluorescent materials and showed that a single shot measurement is sufficient for the decomposition. In contrast to existing methods, this single shot ability allowed for effective operation on complex dynamic scenes as demonstrated in the experiments. In addition, we showed that our method's effective recovery of the direct component greatly improved an existing photometric stereo method. Although we only demonstrated this on the photometric stereo method, our method can be easily applied to any methods that assume direct lighting and a uniform Lambertian surface. In the future, we would like to explore the benefits of separating for dynamic scenes through applications such as dynamic color relighting.

References

1. Achar, S., Nuske, S., Narasimhan, S.G.: Compensating for motion during direct-global separation. In: Proc. of International Conference on Computer Vision (ICCV). pp. 1481–1488 (Dec 2013)
2. Forsyth, D., Zisserman, A.: Mutual illumination. In: Proc. of IEEE Conference on Computer Vision and Pattern Recognition (CVPR). pp. 466–473 (Jun 1989)
3. Forsyth, D., Zisserman, A.: Shape from shading in the light of mutual illumination. Image Vision Computing 8(1), 42–49 (1990)
4. Fu, Y., A., L., Sato, I., Okabe, T., Sato, Y.: Separating reflective and fluorescent components using high frequency illumination in the spectral domain. In: Proc. of International Conference on Computer Vision (ICCV) (2013)

5. Funt, B.V., Drew, M.S., Ho, J.: Color constancy from mutual reflection. International Journal of Computer Vision (IJCV) 6(1), 5–24 (1991)
6. Funt, B., Drew, M.: Color space analysis of mutual illumination. IEEE Trans. Pattern Analysis and Machine Intelligence (PAMI) 15(12), 1319–1326 (1993)
7. Glassner, A.S.: A model for fluorescence and phosphorescence. In: Photorealistic Rendering Techniques, pp. 60–70. Springer Berlin Heidelberg (1995)
8. Han, S., Matsushita, Y., Sato, I., Okabe, T., Sato, Y.: Camera spectral sensitivity estimation from a single image under unknown illumination by using fluorescence. In: Proc. of IEEE Conference on Computer Vision and Pattern Recognition (CVPR) (2012)
9. Hullin, M.B., Fuchs, M., Ihrke, I., Seidel, H.P., Lensch, H.P.A.: Fluorescent immersion range scanning. ACM Trans. on Graph. (ToG) 27, 87:1–87:10 (2008)
10. Hullin, M.B., Hanika, J., Ajdin, B., Seidel, H.P., Kautz, J., Lensch, H.P.A.: Acquisition and analysis of bispectral bidirectional reflectance and reradiation distribution functions. ACM Trans. on Graph. (ToG) 29, 97:1–97:7 (2010)
11. Johnson, G., Fairchild, M.: Full-spectral color calculations in realistic image synthesis. IEEE Computer Graphics and Applications 19, 47–53 (1999)
12. Koenderink, J.J., vanDoorn, A.J.: Geometrical modes as a general method to treat diffuse interreflections in radiometry. Journal of the Optical Soceity of America (JOSA) 73(6), 843–850 (1983)
13. Lakowicz, J.R.: Principles of Fluorescence Spectroscopy. Springer (2006)
14. Lam, A., Sato, I.: Spectral modeling and relighting of reflective-fluorescent scenes. In: Proc. of IEEE Conference on Computer Vision and Pattern Recognition (CVPR) (2013)
15. Liao, M., Huang, X., Yang, R.: Interreflection removal for photometric stereo by using spectrum-dependent albedo. In: Proc. of IEEE Conference on Computer Vision and Pattern Recognition (CVPR). pp. 689–696 (2011)
16. McNamara, G., Gupta, A., Reynaert, J., Coates, T.D., Boswell, C.: Spectral imaging microscopy web sites and data. Cytometry. Part A: the journal of the International Society for Analytical Cytology 69(8), 863–871 (2006)
17. Nayar, S.K., Gao, Y.: Colored interreflections and shape recovery. In: Proceedings of the Image Understanding Workshop (1992)
18. Nayar, S.K., Krishnan, G., Grossberg, M.D., Raskar, R.: Fast separation of direct and global components of a scene using high frequency illumination. In: ACM SIGGRAPH. pp. 935–944 (2006)
19. Nayar, S., Ikeuchi, K., Kanade, T.: Shape from interreflections. International Journal of Computer Vision (IJCV) 6(3), 173–195 (1991)
20. O'Toole, M., Mather, J., Kutulakos, K.N.: 3d shape and indirect appearance by structured light transport. In: Proc. of IEEE Conference on Computer Vision and Pattern Recognition (CVPR) (Jun 2014)
21. Sato, I., Okabe, T., Sato, Y.: Bispectral photometric stereo based on fluorescence. In: Proc. of IEEE Conference on Computer Vision and Pattern Recognition (CVPR) (2012)
22. Sato, I., Zhang, C.: Image-based separation of reflective and fluorescent components using illumination variant and invariant color. IEEE Trans. Pattern Analysis and Machine Intelligence (PAMI) 35(12), 2866–2877 (2013)
23. Seitz, S.M., Matsushita, Y., Kutulakos, K.N.: A theory of inverse light transport. In: Proc. of International Conference on Computer Vision (ICCV). pp. 1440–1447 (2005)
24. Treibitz, T., Murez, Z., Mitchell, B.G., Kriegman, D.: Shape from fluorescence. In: Proc. of European Conference on Computer Vision (ECCV). pp. 292–306 (2012)

25. Wilkie, A., Weidlich, A., Larboulette, C., Purgathofer, W.: A reflectance model for diffuse fluorescent surfaces. In: International conference on Computer graphics and interactive techniques. pp. 321–331 (2006)
26. Woodham, R.J.: Photometric method for determining surface orientation from multiple images. Optical Engineering 19(1) (1980)